A Constitutive Model For Masonry Structures
Practical Application Under Earthquake Loading In Groningen

Panagoulias, S.; Laera, Anita; Vilhar, Gregor; Brinkgreve, Ronald

Publication date
2018

Document Version
Accepted author manuscript

Published in
Proceedings of the 16th European Conference on Earthquake Engineering

A CONSTITUTIVE MODEL FOR MASONRY STRUCTURES: PRACTICAL APPLICATION UNDER EARTHQUAKE LOADING IN GRONINGEN

Stavros PANAGOULIAS[1], Anita LAERA[2], Gregor VILHAR[3], Ronald B.J. BRINKGREVE[4]

ABSTRACT

In this paper, a constitutive model for masonry structures is presented. It is based on the Jointed Rock (JR) model with overall Mohr-Coulomb (MC) failure criterion, and it is implemented as a user-defined soil model in the finite element code PLAXIS. The Masonry model is a linear elastic-perfectly plastic model capable of simulating the macroscopic, anisotropic response of masonry structures, by making use of different potential sliding planes (directions) with different strength properties. A Coulomb criterion is used to simulate failure in each plane, whereas an overall Mohr-Coulomb criterion is used to represent failure of the masonry as a whole. The model is verified against analytical formulations and validated against experimental data. Particular focus is given to its practical application, considering the response of a masonry structure located in Groningen (the Netherlands) under seismic excitation. A soil profile at a specific location between Loppersum and Huizinge is employed, and soil properties are determined based on available geotechnical data. Clayey soil layers are modelled using the Generalised Hardening Soil (GHS) model. Sandy soil layers are modelled with the PM4Sand model. The liquefaction potential is also assessed under certain seismic conditions. The masonry, assumed to be shallow-founded, is subjected to an induced strong ground motion, and its response is studied via the proposed constitutive model.

Keywords: PLAXIS; Masonry; PM4Sand; Liquefaction; Groningen

1. INTRODUCTION

The man-induced earthquakes which occur in the northern part of the Netherlands since the 1990's have been the focus of interest of several researchers and engineers in recent years (Korff et al., 2017; Panagoulias et al., 2017). The unceasing gas field extraction since 1963, lead to ground subsidence and induced seismic actions at shallow depths, approximately three kilometres below the ground surface (https://www.knmi.nl). Their diverse nature, comparing to the natural tectonic earthquakes, in combination with the fact that there is little experience with this specific type of earthquakes, were leading factors in order to establish the Dutch Practice Guideline (NPR) for the assessment of earthquake resistance of various types of structures, newly constructed or existing (NPR 9998:2017).

The Groningen region is moderately populated. The most common type of housing is one to two-storey buildings, mostly composed of unreinforced masonry (URM) (Michalaki, 2015). The majority of these short and brittle structures, with high natural frequencies, are vulnerable to seismic loading. Despite the fact that the induced earthquakes in Groningen are characterised by a low-frequency content (NAM, 2013), the lack of seismic reinforcement, may lead to severe damage or collapse.

This research deals with the elasto-plastic behaviour that the URM develops during monotonic and dynamic loading. The anisotropic nature of the structure is modelled in a macroscopic scale via an elastic perfectly-plastic constitutive model. PLAXIS 2D (2017 version) is used to study the response of a shallow-founded URM structure located in Groningen. The effect of the shallow soft deposits is first investigated via one-

[1]Researcher, Plaxis bv, Delft, the Netherlands, s.panagoulias@plaxis.com
[2]Researcher, Plaxis bv, Delft, the Netherlands, a.laera@plaxis.com
[3]Researcher, Plaxis bv, Delft, the Netherlands, g.vilhar@plaxis.com
[4]Associate Professor, Delft University of Technology, Delft, the Netherlands, R.B.J.Brinkgreve@tudelft.nl

dimensional site response analyses. The liquefaction potential of the selected soil profile is assessed numerically and analytically. The constitutive model PM4Sand (Boulanger and Ziotopoulou, 2017) is used to model the sand layers, while the Generalised Hardening Soil model is used to model the clay layers. Under a non-liquefiable surmise, the response of the superstructure is studied.

2. SOIL CHARACTERISTICS

Geotechnical investigations reveal that soft soil deposits cover the uppermost ten metres in Groningen, mostly consisting of soft clays and peats (Arup, 2015). These soft soil layers cause non-linear site effects and alter the frequency content and the amplitude of the induced seismic ground motion substantially.

2.1 Soil profile

The location of interest was chosen in the region of Westeremden, which is in between Loppersum and Huizinge, in the province of Groningen. Huizinge is the epicentre of the strongest seismic event recorded so far, on August 16th, 2012, with magnitude (M_w) equal to 3.6 (Dost and Kraaijpoel, 2013). The DINOloket web tool (https://www.dinoloket.nl) was used to acquire soil data for the selected location. More specifically, the Cone Penetration Test CPT48434 was employed. In the vicinity of this CPT, the borehole B07E0029 was used to obtain a complete set of soil characteristics. The locations of the CPT and the borehole are illustrated in Figure 1.

Figure 1. Location of the CPT48434 and the borehole B07E0029 (Google Earth Pro, 2017)

Table 1. Soil stratigraphy and parameters (CS: sandy clay; sCS: slightly sandy clay; SC: very clayey sand; SF: extremely fine sand; mSF: medium fine sand).

ID	Stratigraphy	Top (m)	Bottom (m)	γ_{sat} (kN/m^3)	q_c (MPa)	v_s (m/s)	s_u (kN/m^2)	OCR (-)	PI (%)
C1	sCS	0.0	3.0	12.9	0.5	44-81	12-15	2.0	30
S1	SC	3.0	8.0	18.8	3.0	89-170	-	-	-
C2	CS	8.0	10.0	12.9	0.4	112-114	32-34	2.0	30
S2	mSF	10.0	12.0	19.4	12.0	276	-	-	-
C3	sCS	12.0	22.0	17.6	2.0	182-229	94-161	5.5	50
S3	SF	22.0	30.0	19.6	4.5	277-288	-	-	-

The data and correlations provided by Bommer et al. (2017a) were used to estimate the required soil parameters based on the available CPT and borehole data. Table 1 presents the adopted soil stratigraphy and values of various soil parameters, namely, the saturated unit weight (γ_{sat}), the average CPT cone resistance

(q_c), the shear wave velocity (v_s), the undrained shear strength (s_u), the overconsolidation ratio (OCR) and the plasticity index (PI). The soil profile is discretised in six soil layers as listed in Table 1. Provided that the bedrock in Groningen is located deeper than 200.0 m, a half-space is assumed at 30.0 m depth with shear wave velocity of 360 m/s and bulk density of 2.14 t/m^3 (Arup, 2015).

2.2 Calibration of soil parameters

Two advanced constitutive models are employed to model the soil behaviour under dynamic loading conditions, namely the PM4Sand model and the Generalised Hardening Soil model (GHS) model. The PM4Sand model, developed at University of California, Davis (Boulanger and Ziotopoulou, 2017), is a stress-ratio controlled, critical state compatible, bounding surface plasticity model, for simulating the behaviour of sands in dynamic loading, including pore pressure generation and liquefaction. It is an attractive model for practical applications because it can realistically capture cyclic soil response with only a small number of parameters to be calibrated. The PM4Sand model is used to model the sand layers. The primary parameter to be determined is h_{p0}. This parameter influences the contraction rate and, consequently, it determines the number of cycles to liquefaction and can be calibrated based on the Cyclic Resistance Ratio (CRR), which can be obtained from CPT data via empirical correlations (Boulanger and Idriss, 2014).

The GHS model is a generalised form of the Hardening Soil model with small-strain stiffness (Benz, 2007). This model includes a stress and strain-dependent stiffness formulation as well as shear hardening and compaction (cap) hardening in primary loading. Hysteretic damping is a result of the elastic shear modulus reduction formulation, which has a lower bound (maximum damping) when reaching the elastic unloading/reloading shear modulus. The model is not explicitly meant to be used in dynamic applications, but may be used for non-liquefiable soils that do not show significant accumulation of strain or pore pressure during cyclic loading. The GHS model is used to model the clay layers. For this work, the stress-dependent stiffness is kept constant during the calculation phase, based on the stresses at the beginning of the calculation.

Besides the soil data provided by Bommer et al. (2017a), empirical correlations (Lunne et al., 1997) are applied to estimate the remaining model parameters. Table 2 summarises the selected values. Default values are used for the secondary parameters of the PM4Sand model (Boulanger and Ziotopoulou, 2017).

Table 2. Model parameters of the GHS model for the clay layers C1, C2 and C3 and the PM4Sand model for the sand layers S1, S2 and S3 (DT: drained triaxial test; OED: oedometer test).

Parameter	**Symbol**	**Unit**	**Value**					
			C1	**C2**	**C3**	**S1**	**S2**	**S3**
Secant stiffness (DT)	E_{50}^{ref}	kN/m^2	1.9E3	2.4E3	16.3E3	-	-	-
Tangent stiffness (OED)	E_{oed}^{ref}	kN/m^2	1.5E3	1.9E3	13.0E3	-	-	-
Un/re-loading stiffness (DT)	E_{ur}^{ref}	kN/m^2	5.7E3	7.2E3	48.9E3	-	-	-
Power of stiffness stress dependency	m	-	0.80	0.85	0.80	-	-	-
Effective cohesion	c'_{ref}	kN/m^2	3.0	7.0	19.0	-	-	-
Effective friction angle	φ'	deg	22.0	25.0	29.0	-	-	-
Dilatancy angle	ψ	deg	0.0	0.0	0.0	-	-	-
Threshold shear strain	$\gamma_{0.722}$	-	0.4E-3	0.4E-3	0.8E-3	-	-	-
Small-strain shear modulus	G_0^{ref}	kN/m^2	37.0E3	40.0E3	68.0E3	-	-	-
Poisson's ratio	ν'_{ur}	-	0.2	0.2	0.2	-	-	-
Reference stress	p_{ref}	kN/m^2	100.0	100.0	100.0	-	-	-

Failure ratio	R_f	-	0.9	0.9	0.9	-	-	-
Tensile strength	σ_t	kN/m^2	0.0	0.0	0.0	-	-	-
Apparent relative density	D_{R0}	-	-	-	-	0.50	0.85	0.50
Shear modulus coefficient	G_0	-	-	-	-	670	1830	1160
Contraction rate parameter	h_{p0}	-	-	-	-	0.50	0.90	0.22
Lateral stress ratio	K_0	-	0.5	0.5	1.1	0.5	1.0	1.0

3. INPUT GROUND MOTIONS

The NEN web tool (http://seismischekrachten.nen.nl/webtool.php) was used to obtain the elastic response spectrum and the peak ground acceleration (PGA), in accordance with the NPR 9998:2017, at the vicinity of the location of interest (latitude 53°20'19.2"N, longitude 6°42'16.5"E). The return period is taken equal to 475 years, which corresponds to a 10% probability of exceedance in 50 years. The corresponding PGA equals 0.19 g. The maximum most-probable expected moment magnitude (M_w) is taken equal to 4.5 (Bommer and van Elk, 2017; Bommer et al., 2017b).

The ground motions provided by NPR 9998:2015 are used for the non-linear dynamic time analysis. Note that during the preparation of this research, the NEN web tool did not provide any updated accelerograms, contrary to what was indicated by NPR 9998:2017. In total eleven time histories are available, spectrally matched to the 2016 NPR target design spectrum at 30.0 m depth. The time signals are linearly scaled to the PGA of 0.19 g. Figure 2 depicts the eleven time signals, together with the adopted code names. All of the selected signals are acting in the horizontal x-direction.

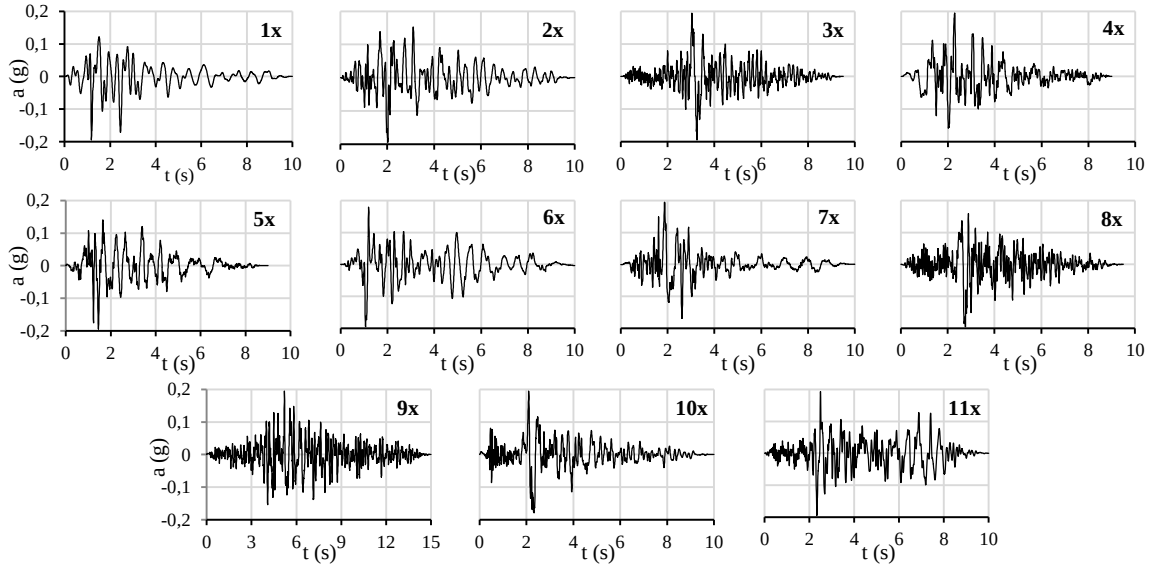

Figure 2. Time signals scaled to a PGA of 0.19 g (after NPR 9998:2015)

4. LIQUEFACTION EVALUATION

The liquefaction potential of the selected soil profile, under the seismic conditions described in Section 3, is studied via site response analyses (SRA). Only horizontal excitation in the x-direction is considered. A vertical soil column with a depth equal to 31.0 m (the bottom 1.0 m is used to model the half-space) is excited horizontally under plane strain two-dimensional conditions. Half-space properties are determined after Arup (2015). The width of the model is set equal to 1.0 m, selected such that the average length of the

mesh elements is less than one-eighth of the maximum input wavelength (Kuhlemeyer and Lysmer, 1973). "Tied degrees of freedom" are employed as dynamic side model boundaries, whereas a "Compliant base" is used at the bottom of the model. To consider only the upward propagating motion of the shear waves, half the amplitude of the input seismic motion is taken into account. The K_0 procedure is used to initiate the soil stress state (Brinkgreve et al., 2017). The phreatic level is set to ground surface.

The model parameters presented in Table 2 are used for the analyses. Rayleigh damping is taken into account for all soil layers, following the approach proposed by Hudson et al. (1994). The selected values equal 1.3 Hz for the first target frequency (f_1) and 3.0 Hz for the second target frequency (f_2), and the target damping ratio reads 1%, leading to Rayleigh damping coefficients α_R and β_R of 0.1140 and 0.7403E-3 respectively. Based on the number of data points in the earthquake signal, the dynamic calculation was performed in 2000 steps with 10 substeps using the undamped Newmark implicit time integration scheme.

Attention is paid to the numerical results regarding the maximum excess pore pressure ratio $r_{u,max}$ and the maximum shear strain, per sand soil layer. For all time histories, the top sand layer (S1) is considered liquefiable as $r_{u,max}$ is nearly equal to 1.0, and the obtained shear strain varies between 1% and 2%. Concerning the second sand layer (S2), no liquefaction potential is observed as $r_{u,max}$ does not exceed 0.1, and the maximum shear strain is in the range of 0.01%. With respect to the bottom sand layer (S3), limited liquefaction potential is noticed as $r_{u,max}$ equals 0.2 on average, while it reaches a maximum value of 0.5 for the time signal 6x (Figure 2). The maximum shear strain is less than 0.1%.

The numerical results are compared with the semi-empirical method presented by Boulanger and Idriss (2014). The factor of safety (FoS), on average along the depth of each soil layer, equals 0.7 for the top sand layer (S1), 6.0 for the mid sand layer (S2) and 1.6 for the bottom sand layer (S3), giving confidence to the numerical-based conclusions.

5. THE MASONRY CONSTITUTIVE MODEL

The Masonry model (Amorosi et al., 2015; Amorosi et al., 2018), is based on the anisotropic Jointed Rock constitutive model and implemented as a user-defined soil model in PLAXIS. It is a linear elastic-perfectly plastic model aimed to simulate the macroscopic, anisotropic response of URM structures (block structures with periodic texture). A Coulomb criterion is employed to simulate failure in predefined failure directions (failure planes), whereas an overall Mohr-Coulomb criterion is used to represent a failure of the masonry blocks.

Due to the specific form that the unit blocks are placed in horizontal layers, the tensile and shear strength along the head joints (noted as direction 1-1') is enhanced due to the contribution of the bed joints (noted as direction 2-2'), which are subjected to an increasing vertical stress state (Figure 3). The model is formulated such that both tensile and shear strength increase as a function of depth, as given by Equations 1 to 3. The first term represents the regular cohesive and tensile strength of the head joints, while the second and third terms correspond to the frictional and cohesive contributions of the bed joints accordingly. Both last terms account for the interlocking effects. No modifications are introduced for the plane parallel to the bed joints as, due to geometrical reasons, no interlocking effects are developed along that plane.

$$c_{1,mod} = c_1 - SF_{beta} \cdot \sigma_{(1,2)} + c_2 \cdot SF_{beta} / \tan\varphi_2 \quad (1)$$

$$\sigma_{t1,mod} = \sigma_{t1} - SF_{beta} \cdot \sigma_{(1,2)} + c_2 \cdot SF_{beta} / \tan\varphi_2 \quad (2)$$

$$SF_{beta} = \tan\varphi_2 \cdot b / (2a) \quad (3)$$

in which, a is the block's height, b is the block's width, $\sigma_{(1,2)}$ is the stress acting perpendicular to the bed joints (compression is negative), c_1 is the cohesion acting on plane 1-1', c_2 the cohesion acting on plane 2-2' and $\tan\varphi_2$ the friction coefficient of plane 2-2' (Figure 3).

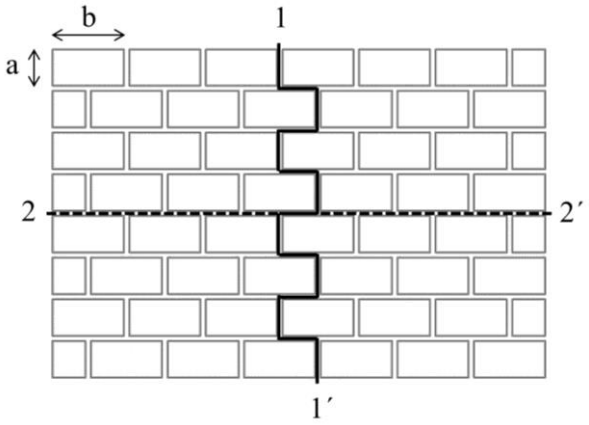

Figure 3. Head (1-1') and bed (2-2') joints direction of a masonry wall

5.1 Model parameters and calibration

Six parameters are employed to model the stiffness and the strength of the masonry as a continuum, namely, shear modulus G, Poisson's ratio ν, cohesion c_{mc}, friction angle φ_{mc}, dilation angle ψ_{mc} and tensile strength $\sigma_{t,mc}$. Four additional strength parameters are used for the head and bed joints respectively, namely, cohesion c_1 and c_2, friction angle φ_1 and φ_2, dilation angle ψ_1 and ψ_2 and tensile strength σ_{t1} and σ_{t2}.

The isotropic elastic model parameters G and ν are related to the overall response of the structure. In case that elastic properties of the units and the joints are used, a homogenisation procedure should be considered (de Felice et al., 2010), to obtain an anisotropic continuum based formulation. This procedure is elaborated in the Appendix.

5.2 Model verification and validation

5.2.1 Static traction test

A masonry panel is studied, subjected to self-weight, vertical pressure applied on top and tensile strain on the lateral sides. The lateral tensile strain is applied in the form of a horizontal prescribed displacement up to failure. The structure is 3.0 m long, 0.98 m high and 0.12 m wide in the out-of-plane direction (Figure 4a). Due to symmetry, only half of the model is considered under two-dimensional plane strain conditions, while the finite element mesh is composed of 580 15-noded triangular elements.

Table A.1 gives the geometrical and mechanical model parameters, determined after de Felice et al. (2010). High values are assigned to the cohesion and tensile strength of the blocks to force the failure mechanism to be formed along the sliding planes. The tensile strength of both sliding planes is determined by the Mohr-Coulomb failure criterion. An associated plastic flow rule is assumed. The unit weight of the structure is taken equal to 15.0 kN/m^3, and the applied vertical pressure (q) equals 10.0 kPa.

The analytical solution of the maximum horizontal traction T_{max} is given by Equation 4 (de Felice et al., 2010), where H is the height of the structure.

$$T_{max} = H \cdot (c / \tan\varphi + c \cdot SF_{beta} / \tan\varphi + \gamma \cdot H \cdot SF_{beta} / 2 + q \cdot SF_{beta}) \quad (4)$$

Figure 4b illustrates a comparison between the numerical results obtained from the Masonry model and the analytical solution given by Equation 4. The results indicate excellent agreement, with T_{max} equal to 25.43 kN/m.

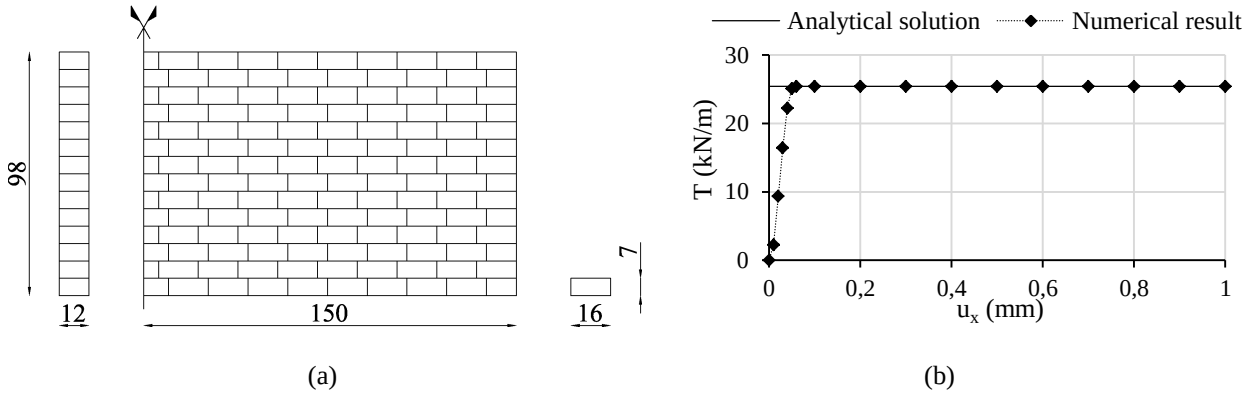

Figure 4. Geometric dimensioning (distances in mm) of the experimental setup (a) and tensile strength test results (b)

5.2.2 Static shear tests

Two masonry walls, one with and one without opening, are studied in this validation example. The panels have dimensions of 0.99 x 1.0 x 0.1 m^3 (Figure 5a). The opening has dimensions of 0.235 x 0.4 x 0.1 m^3 (Figure 5b). They consist of wire-cut solid clay bricks with dimensions 210 x 52 x 100 mm^3 (Raijmakers and Vermeltfoort, 1992). The walls are first subjected to their self-weight (15.0 kN/m^3), and a vertical pressure of 300.0 kPa is applied subsequently. Shearing is applied via a horizontal displacement distributed along the top boundary of the walls, inhibiting rotation. For the walls with and without opening, the finite element mesh is composed of 1050 and 1040 15-noded triangular elements respectively.

Table A.1 presents the mechanical material parameters, determined after Raijmakers and Vermeltfoort (1992). The elastic shear modulus G is derived from the homogenisation procedure and its value is in agreement with the value used by Pelà et al. (2013).

Figures 6a and 6b depict the numerically obtained results in comparison with the experimental data in terms of load-displacement curves. It is concluded that the results are in good agreement. The formulation of the Masonry model does not account for strength reduction along the joints. Consequently, the model can capture sufficiently the ultimate strength of the structure but not the strain-softening behaviour (decreasing strength) measured from the experiments.

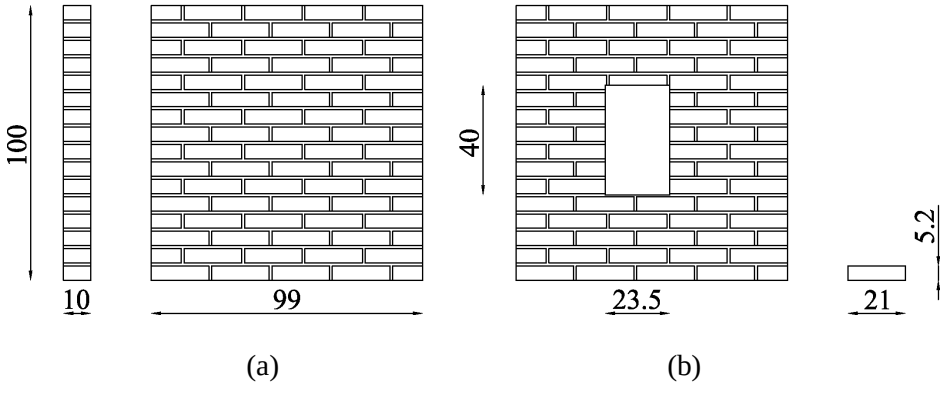

Figure 5. Geometric dimensioning (distances in mm) of the wall without (a) and with opening (b)

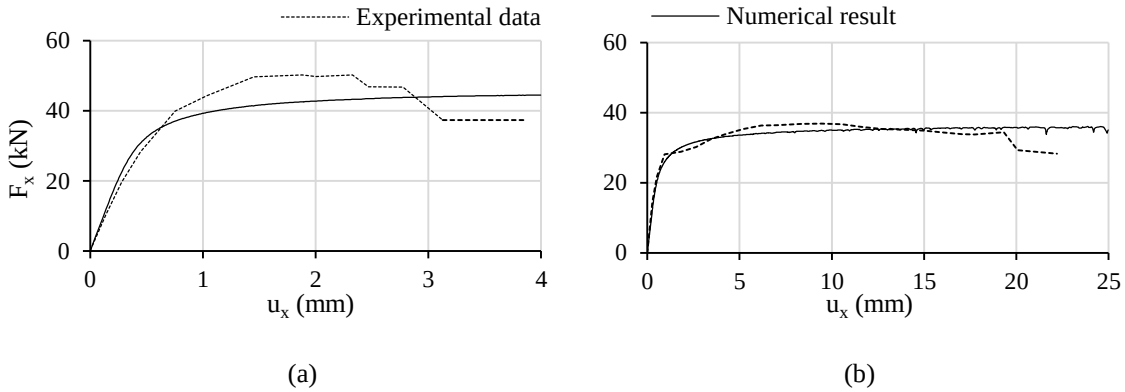

Figure 6. Shear strength test results for a wall without (a) and with opening (b)

5.2.3 Cyclic shear test

An in-plane cyclic shear test of a slender masonry pier made of calcium silicate blocks is considered for this verification example. A 1.25 m long, 2.5 m high and 0.175 m thick full-scale wall was subjected to lateral quasi-static cyclic loading under controlled double-bending boundary conditions. The tests were carried out at the EUCENTRE laboratory under the auspices of the ESECMaSE research project (http://www.esecmase.org/). The experimental results from the CS05 wall (Magenes et al., 2008) are compared with the numerical results obtained from the Masonry model.

A two-dimensional plane strain model is used. The finite element mesh consists of 900 15-noded triangular elements. The bottom of the model is fully fixed, while rotation of both top corner points is prevented to simulate a double-bending boundary condition. Both head and bed joints are filled with a thin layer of mortar. Table A.1 presents the selected material parameters. The wall is first subjected to vertical compression stress of 1.0 MPa. Displacement-controlled cyclic shearing is subsequently applied to the top boundary. The imposed horizontal displacement history is determined after Magenes et al. (2008), illustrated in Figure 7a. The maximum imposed displacement in the numerical analysis reads 10 mm. This value is lower than the displacement imposed in the experiments (Figure 7b), but it is considered high enough to study the behaviour of the numerical model and to draw conclusions. Rayleigh damping of 1.0% was employed at target frequencies of 1.0 Hz and 30.0 Hz (Grant et al., 2015).

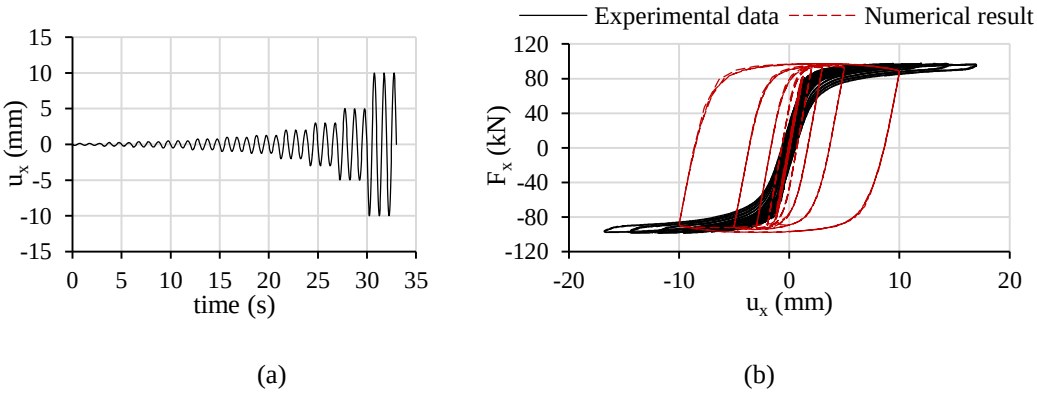

Figure 7. Imposed horizontal displacement time history (a) and force-displacement curves (b) for the wall CS05

Figure 7b depicts the comparison between the experimental and the numerical results by means of force-displacement curves. The numerical model can capture the strength capacity of the pier decently up to the point that yielding occurs. Assuming that failure conditions are met when the maximum shear strength is reached, the post-failure behaviour cannot be appropriately captured by the numerical model. The experiments reveal a bending-rocking behaviour of the pier, while the numerical results indicate significantly higher energy dissipation. This difference is possibly caused by the early damage that occurred in the

numerical model and the inability to consider cracks closure during unloading and reloading, releasing more energy than the rocking behaviour of the full-scale wall.

6. CASE STUDY

The present case study focuses on the performance of a URM structure, founded on the soil profile presented in Section 2.1, under plane strain conditions. A horizontal in-plane seismic excitation is used, with a lower PGA value, equal to 0.10 g (return period of 95 years), to study the response of the superstructure under non-liquefaction conditions. Such a loading scenario is more likely to occur and is assumed to be more critical for the structural response.

In a practical case for which a complete design study should be performed, all eleven time signals presented in Section 3 should be preferably used (NPR 9998:2017). However, the purpose of this case study is to demonstrate the use of the Masonry model in combination with advanced soil constitutive models. Only the results of the numerical analysis with the ground motion 1x (Figure 2) as input earthquake signal, linearly scaled to a PGA of 0.10 g, are discussed, under the assumption that the adopted approach constitutes a representative seismic scenario for the present case study.

A typical two-storey Dutch residence made of URM is employed. The layout of the building is selected after Michalaki (2015). The mechanical parameters are chosen assuming poor quality clay brickwork with construction year before 1945 (NPR 9998:2017). The Masonry model parameters are determined following the homogenization procedure described in the Appendix. The selected values are presented in Table A.1. The Rayleigh damping coefficients α_R and β_R for the masonry structure are equal to 0.5712 and 1.447E-3 correspondingly, such that 5% damping (according to NPR 9998:2017) corresponds to target frequencies of 1.0 Hz and 10.0 Hz. The building is assumed shallow founded. A concrete slab is modelled via a linear elastic non-porous material, up to 0.5 metres below ground surface. Imposed loads, equal to 9.0 kN/m/m (CEN, 2002), are modelled as distributed masses via zero-stiffness beam elements at the level of the first and second floor. The structure is depicted in Figure 8b.

The water table is assumed at ground surface level. The liquefaction potential is examined both analytically and numerically, and it is ensured that, under the studied seismic conditions, liquefaction is not likely to occur. Drained conditions are considered for the initiation of stresses, whereas an undrained dynamic analysis is employed for the seismic event.

“Free field” boundary conditions are used as dynamic side model boundaries, which are extended to 90.0 m from the model centreline to minimise wave reflections. A “Compliant base” is used at the bottom of the model. The finite element mesh consists of 7942 15-noded triangular elements, and it is locally refined within and around the superstructure, to capture any developed failure mechanisms. Figure 8a illustrates part of the model, focusing on the vicinity of the structure. The dynamic calculation was performed in 2000 steps with 10 substeps using the undamped Newmark implicit time integration scheme.

Figure 9a illustrates the stress points that have been in failure condition throughout the entire dynamic analysis, indicated with brown marks. They are mainly located at the openings and the piers of the second floor. Figure 9b shows the total deviatoric strains developed on the superstructure during the seismic excitation, at the peak deviatoric strains demand (2.765 s). The maximum value reads about 0.03% concentrated at the corner regions of the openings of the second floor, emphasised in the black circles in Figure 9b. The deviatoric strains captured on the ground floor are primarily elastic as indicated from the limited failure stress points at that area (Figure 9a), and the fact that they are one order of magnitude lower than the plastic deviatoric strains developed on the first floor.

Despite the fact that a conservative approach of poor quality construction, resulting in lower values of material strength and stiffness, was adopted, the masonry underwent limited damage under the presented earthquake scenario. The observed total deviatoric strains and failure stress points indicate that the structure stays almost intact and safe. As indicated in Section 5.2.3, the Masonry model may sufficiently capture the

structural response up to the point that the strength capacity is reached, assuring a reliable performance of the structure. Beyond that state, the computed structural response may not be realistic. In the present case study, the superstructure is subjected to overall limited damage, without indication of global failure. It is concluded that no significant overestimation of energy dissipation occurs and the numerical results are credible.

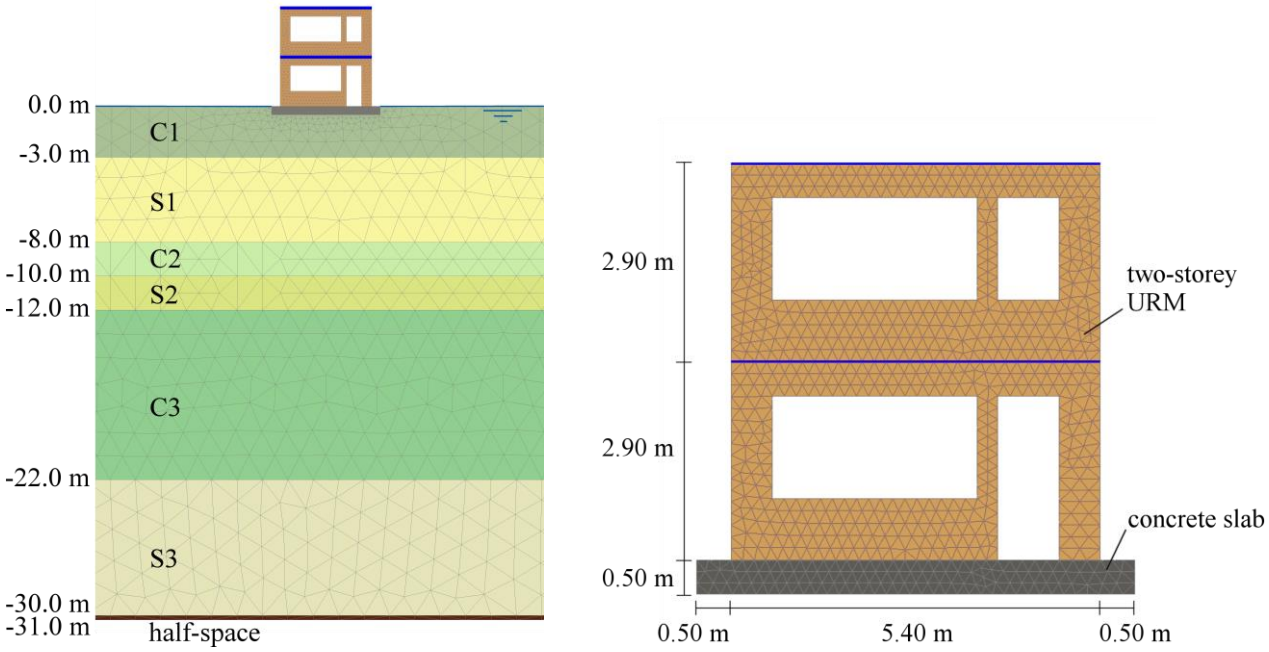

(a) (b)

Figure 8. Part of the model geometry and the finite element mesh in the vicinity of the superstructure (a), and primary dimensions and the finite element mesh of the masonry structure (b)

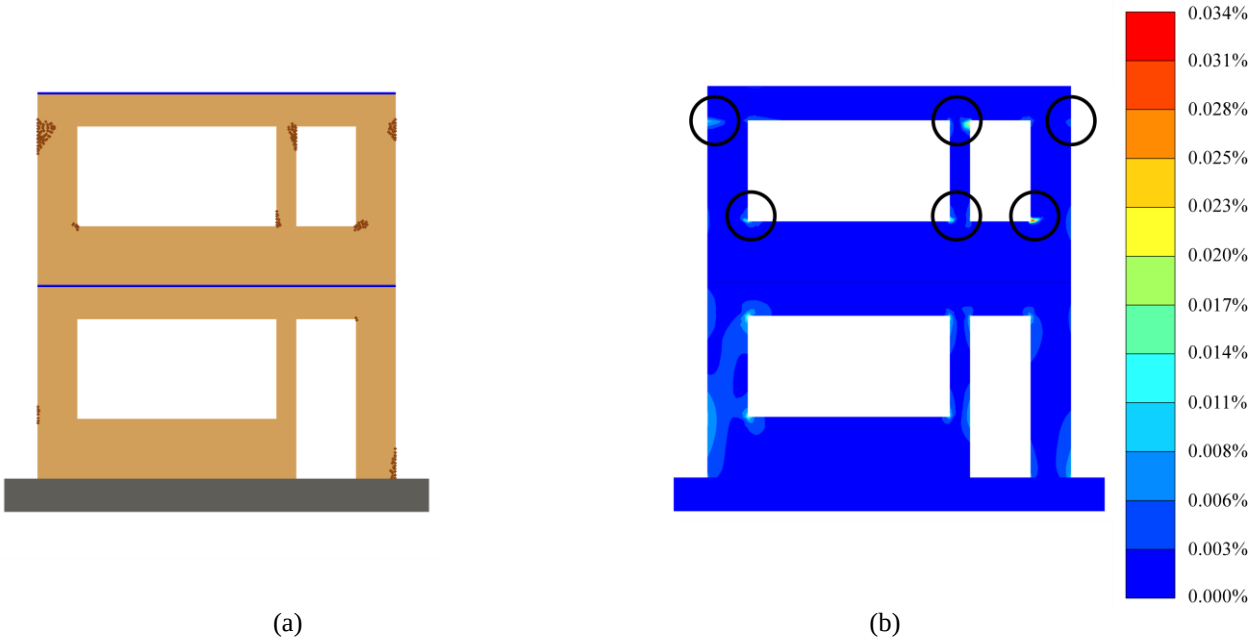

(a) (b)

Figure 9. Stress points at failure throughout the dynamic analysis (a) and total deviatoric strains (b) at the peak deviatoric strains demand (2.765 s)

7. CONCLUDING REMARKS

The liquefaction potential in Groningen is evaluated focusing on a specific soil profile located close to the epicentre of the strongest seismic event recorded so far in this region, namely, the Huizinge earthquake. For this purpose, the PM4Sand constitutive model is employed. The model can genuinely simulate cyclic soil response and assess liquefaction, by calibrating only a limited number of parameters. Under the assumption of a seismic event with return period equal to 475 years, liquefaction is found to be a valid hazard for the top sand layer. The soundness of the numerical results is checked against semi-empirical analytical formulations.

A constitutive model for URM structures is presented in this research.The Masonry model is implemented in a geotechnical finite element analysis software in a three-dimensional framework and may be efficiently used for ground response problems together with sophisticated soil constitutive models, which can simulate the soil-structure interaction under dynamic loading conditions. This is demonstrated via a practical case, in which the response of a URM structure is studied. A seismic event with a return period of 95 years is assumed to establish a non-liquefaction regime. Such seismic scenario is more likely to occur, and it is thought to be more critical for the structural performance, comparing to a case that liquefaction would take place. The numerical results indicate that the superstructure remains relatively undamaged during the dynamic analysis, giving confidence to the adequate seismic response of a typical residence in Groningen, under the presumed soil and seismic conditions.

The Masonry model is also verified and validated against analytical and experimental results. It is demonstrated that the model can adequately reproduce the interlocking mechanism which is developed between the masonry unit blocks during loading. Failure mechanisms such as tensile cracks which propagate downwards are often observed on masonry structures and may be attributed to this mechanism. The model is capable of predicting the shear and tensile strength of the masonry structures under static and cyclic loading, which is a primary concern of all practical applications. Under cyclic loading conditions, the model may not sufficiently capture the response of the structure after the point that the ultimate strength capacity is reached and cracking is initiated. The latter constitutes a topic of further research and development.

8. ACKNOWLEDGMENTS

The authors gratefully acknowledge the cooperation with Assoc. Prof. A. Amorosi, Assoc. Prof. D. Boldini, Prof. G. de Felice, Dr M. Malena and Ms W.G. Lasciarrea for the development and validation of the Masonry constitutive model.

9. REFERENCES

Amorosi A, Boldini D, de Felice G, Lasciarrea WG, Malena M (2015). Analisi geotecnica e strutturale del Ninfeo di Genazzano. *Rivista Italiana di Geotecnica*, 49(1), 29-44.

Amorosi A, Boldini D, de Felice G, Lasciarrea WG, Malena M. (2018). Jointed Masonry Model: a new versatile constitutive law for 3D analysis of masonry structures. *Submitted for publication*.

Arup (2015). Groningen Earthquakes Structural Upgrading, Site Response Analysis. Arup report 229746, Amsterdam, the Netherlands.

Benz T (2007). Small-strain stiffness of soils and its numerical consequences. *PhD Thesis*, Institut für Geotechnik, Universität Stuttgart, Stuttgart, Germany.

Bommer JJ, van Elk J (2017). Comment on "The Maximum Possible and the Maximum Expected Earthquake Magnitude for Production-Induced Earthquakes at the Gas Field in Groningen, The Netherlands" by Gert Zöller and Matthias Holschneider. *Bulletin of the Seismological Society of America*, 107: 1564-1567, doi: 10.1785/0120170040.

Bommer JJ, Dost B, Edwards B, Kruiver PP, Meijers P, Ntinalexis M, Rodriguez-Marek A, Ruigrok E, Spetzler J, Stafford PJ, van Elk J (Ed.), Doornhof D (Ed.) (2017a). V4 Ground-Motion Model (GMM) for Response Spectral Accelerations, Peak Ground Velocity, and Significant Durations in the Groningen Field. Nederlandse Aardolie Maatschappij (NAM), 23 June 2017.

Bommer JJ, Dost B, Edwards B, Kruiver PP, Meijers P, Ntinalexis M, Rodriguez-Marek A, Ruigrok E, Spetzler J, Stafford PJ (2017b). V5 Ground-Motion Model (GMM) for the Groningen Field. Nederlandse Aardolie Maatschappij (NAM), 30 October 2017.

Boulanger RW, Idriss IM (2014). CPT and SPT based liquefaction triggering procedures. Center for Geotechnical Modeling, Department of Civil and Environmental Engineering, University of California, Davis, CA. Report No. UCD/CGM-14/01.

Boulanger RW, Ziotopoulou K (2017). PM4Sand (Version 3): A sand plasticity model for earthquake engineering applications. *Report No. UCD/CGM-17/01*. Department of Civil & Environmental Engineering, College of Engineering, the University of California at Davis.

Brinkgreve RBJ, Kumarswamy S, Swolfs WM (2017). PLAXIS Material models manual 2017. Plaxis bv, Delft, the Netherlands.

CEN (2002). Eurocode 1 - Actions on structures. Part 1-1: General actions - Densities, self-weight, imposed loads for buildings. EN 1991-1-1:2002. European Committee for Standardization (CEN), Brussels.

Dost B and Kraaijpoel D (2013). The August 16, 2012 earthquake near Huizinge (Groningen). Royal Netherlands Meteorological Institute (KNMI), January 2013.

de Felice G, Amorosi A, Malena M (2010). Elasto-plastic analysis of block structures through a homogenization method. *Int. J. Numer. Analyt. Methods Geomechanics*, 34(3):221-247.

Google Earth Pro (2017). Version 7.3.0.3832 (32-bit). Latitude 53°20'3.03"N, longitude 6°42'1.95"E. Location accessed 29/11/2017.

Grant D, Magenes G, Rots J, van Elk J (Ed.), Doornhof D (Ed.) (2015). Groningen Earthquakes – Structural Upgrading URM Modelling and Analysis Cross-Validation. Nederlandse Aardolie Maatschappij (NAM), 7 July 2015.

Hudson M, Idriss IM, Beikae M (1994). User's manual for QUAD4M. Center for Geotechnical Modeling, Department of Civil and Environmental Engineering, University of California, Davis, California, USA.

Korff M, Wiersma A, Meijers P, Kloosterman F, de Lange G, van Elk J, Doornhof D (2017). Liquefaction Mapping for Induced Seismicity based on geological and geotechnical features. *Proceedings of the 3rd International Conference on Performance-based Design in Earthquake Geotechnical Engineering*, 16-19 July 2017, Vancouver, Canada.

Kuhlemeyer RL, Lysmer J (1973). Finite element method accuracy for wave propagation problems. *J. Soil Mech. and Found. Dev.*, 99(5):421–427.

Lunne T, Robertson PK, Powell JJM (1997). Cone Penetration Testing in Geotechnical Practice. Spon Press, Taylor & Francis Group, London and New York.

Magenes G, Morandi P, Penna A (2008). In-plane cyclic tests of calcium silicate masonry walls. *Proceedings of the 14th International Brick and Block Masonry Conference*, 13-20 February 2008, Sydney, Australia.

Michalaki M (2015). Seismic Assessment of a Typical Dutch Rijtjeshuis. *MSc thesis*, Department of Civil Engineering and Geosciences, Delft University of Technology, Delft, the Netherlands.

NAM (2013). Technical Addendum to the Winningsplan Groningen 2013; Subsidence, Induced Earthquakes and Seismic Hazard Analysis in the Groningen Field. Nederlandse Aardolie Maatschappij (NAM), November 2013.

NPR 9998:2015 (2015). Beoordeling van de constructieve veiligheid van een gebouw bij nieuwbouw, verbouw en afkeuren – Grondslagen voor aardbevingsbelastingen: geïnduceerde aardbevingen. Nederlands Normalisatie Instituut (NEN), Delft, the Netherlands, December 2015.

NPR 9998:2017 (2017). Assessment of structural safety of buildings in case of erection, reconstruction and disapproval - Basic rules for seismic actions: induced earthquakes. English draft. Nederlands Normalisatie Instituut (NEN), Delft, the Netherlands, June 2017.

Panagoulias S, Laera A, Brinkgreve RBJ (2017). A practical study on the induced seismicity in Groningen and the seismic response of a masonry structure. *Proceedings of the 3rd International Conference on Performance-based Design in Earthquake Geotechnical Engineering*, 16-19 July 2017, Vancouver, Canada.

Pelà L, Cervera M, Roca P (2013). An orthotropic damage model for the analysis of masonry structures. *J. of Construction and Building Materials*, 41:957-967.Raijmakers TM, Vermeltfoort ATh (1992). Deformation controlled tests in masonry shear walls. *Report B-92-1156*, TNO-Bouw, Delft, the Netherlands.

APPENDIX

The homogenisation procedure proposed by de Felice et al. (2010), to obtain an anisotropic continuum based formulation, is presented in this Appendix. The shear modulus G is given by Equation A1, while the Poisson's ratio ν is obtained as an average value from Equation A2.

$$1 / G = 1 / (a \cdot K_t) + 4a / (b^2 \cdot K_n + 4a \cdot b \cdot K_t) + 1 / \mu_b \quad (A1)$$

$$\nu_{12} / E_1 = \nu_{21} / E_2 = \lambda'_b / [4\mu_b \cdot (\lambda'_b + \mu_b)] \quad (A2)$$

where ν_{12}, ν_{21} are the Poisson's ratios for the head joints (direction 1-1') and bed joints (direction 2-2') accordingly (Figure 3). The normal joint stiffness K_n is given by Equation A3 and the shear joint stiffness K_t is calculated by Equation A4. The Lame's coefficients μ_b and λ'_b for the unit blocks are given by Equations A5 and A6 respectively. The Young's moduli of the head (E_1) and bed (E_2) are calculated by Equations A7 and A8.

$$K_n = E_b \cdot E_m / [t_m \cdot (E_b - E_m)] \quad (A3)$$

$$K_t = E_b \cdot E_m / [4(1 + \nu_b) \cdot (1 + \nu_m) \cdot t_m \cdot \{E_b / [2(1 + \nu_b)] - E_m / [2(1 + \nu_m)]\}] \quad (A4)$$

$$\mu_b = E_b / [2(1 + \nu_b)] \quad (A5)$$

$$\lambda'_b = \nu_b \cdot E_b / (1 - \nu_b^2) \quad (A6)$$

$$1 / E_1 = 1 / (a \cdot K_n) + 1 / (4\mu_b) + 1 / [4(\lambda'_b + \mu_b)] \quad (A7)$$

$$1 / E_2 = 4a / (4a \cdot b \cdot K_n + b^2 K_t) + 1 / (4\mu_b) + 1 / [4(\lambda'_b + \mu_b)] \quad (A8)$$

in which, E_b is the Young's modulus of the blocks, E_m is the Young's modulus of the mortar, ν_b is the Poisson's ratio of the blocks and ν_m is the Poisson's ratio of the mortar.

Table A1 presents the parameters of the Masonry model used for the numerical simulations of the verification and validation tests presented in Section 5.2, and the study case discussed in Section 6.

Table A1. Masonry model parameters for the tensile strength test (TS), the shear strength tests (SS), the cyclic shear test (CS) and the study case (SC).

Symbol	Unit	Value per test			
		TS	SS	CS	SC
γ	kN/m^3	15.0	15.0	18.0	18.6
G	kN/m^2	0.477E6	1.404E6	2.40E6	0.89E5
ν	-	0.12	0.06	0.112	0.21
c_{mc}	kN/m^2	10.0E6	10.0E6	6380.0	1649.0
φ_{mc}, ψ_{mc}	deg	31.0	36.9	34.0	24.2
$\sigma_{t,mc}$	kN/m^2	10.0E6	10.0E6	2240.0	3664.0
SF_{beta}	-	0.687	1.514	0.1	0.75
φ_1, φ_2, ψ_1, ψ_2	deg	31.0	36.9	34.0	31.0
c_1, c_2	kN/m^2	5.0	350.0	350.0	180.0
σ_{t1}	kN/m^2	8.32	250.0	240.0	210.0
σ_{t2}	kN/m^2	8.32	250.0	240.0	60.0